Lasers in Surgery and Medicine 14:258–268 (1994)

Temperature Dependence of the Absorption Coefficient of Water for Midinfrared Laser Radiation

E. Duco Jansen, MSc, Ton G. van Leeuwen, PhD, Massoud Motamedi, PhD, Cornelius Borst, MD, PhD, and Ashley J. Welch, PhD

Biomedical Engineering Program, University of Texas, Austin, Texas 78712 (E.D.J., A.J.W.); Department of Cardiology, Utrecht University Hospital and Interuniversity Cardiology Institute of the Netherlands, Utrecht, The Netherlands (T.G.v.L., C.B.); Laser and Spectroscopy Laboratory, University of Texas Medical Branch, Galveston, Texas 77555 (M.M.)

The dynamics of the water absorption peak around 1.94 μm was examined. This peak is important for the absorption of holmium and thulium laser radiation. To examine the effect of temperature on the absorption coefficient, the transmission of pulsed Ho:YAG, Ho:YSGG, and Tm:YAG laser radiation through water of 22°C, 49°C, and 70°C was measured as a function of the thickness of the water layer. From these data the absorption coefficients were determined at the three wavelengths. We found that at all three wavelengths, the absorption coefficients decreased when increasing the temperature. Second, the absorption spectrum of water was measured from 1,850–2,150 nm with a spectrophotometer. It was found that the absorption peak at 1.94 μm (at 22°C) shifts to shorter wavelengths with increasing temperatures, to 1.92 μm at 70°C.

A model was developed to predict the temperature distribution incorporating the dynamic change in absorption coefficient. The temperature distributions are compared to the predictions of a model assuming constant optical properties. It is shown in this study that the dynamics of the absorption coefficient has a significant influence on the expected zone of damage and ablation parameters in the 2-μm wavelength range.

Key words: dynamic optical properties, holmium laser, thulium laser, temperature

INTRODUCTION

Pulsed midinfrared lasers are used clinically for the photo ablation of biological tissue. Many reports have described the use of holmium:YAG, holmium:YSGG, and thulium:YAG lasers in medical specialties such as cardiology [1,2], orthopedic surgery [3–5], ophthalmology [6], and ENT surgery [7,8]. There is a general understanding that the infrared ablation mechanism is a process of water vaporization and subsequent photo thermal disruption of tissue [9,10]. In tissue, the main absorber of infrared radiation is water, which is heated and vaporized. This process is typically associated with a rapid subsurface pressure buildup and possible superheating. We and others have used time-resolved flash photography to reveal the formation of a water vapor cavity induced by the laser pulse [10–13].

In situations where the fluence is too low to induce bubble formation or when a very short laser pulse is delivered and bubble formation takes place only after the energy has all been deposited, the initial temperature distribution, assuming no heat conduction is:

Accepted for publication October 22, 1993.

Address reprint requests to E. Duco Jansen, Biomedical Engineering Program, ENS 614A, University of Texas, Austin, TX 78712.

$$\Delta T(z) = \frac{\mu_a Q_0 e^{-\mu_a z}}{\rho c A} \quad (1)$$

where $\Delta T(z)$ [°C] represents the one-dimensional temperature distribution, z is the depth [mm], A is the area [mm^2], and Q_0 is the incident energy [mJ].

In general, the light distribution in the medium in which laser light is deposited is defined by the optical properties (i.e., effective scattering and absorption coefficients, μ_s' and μ_a). In the 2-μm range, the effective scattering coefficient is much smaller than the absorption coefficient ($\mu_s' << \mu_a$) [14]. Hence, the prediction of depth of penetration, temperature distribution, ablation rate, and thermal damage zone is only as good as the used value of the absorption coefficient. In particular, thermal damage caused by denaturation of tissue in the bottom and sides of the ablation crater is of considerable clinical interest, since it can affect the speed of wound healing or may damage critical structures. The simplest thermal models use the optical properties to calculate the depth to which the tissue is heated to the some critical temperature that causes thermal coagulation. Schomacker et al. [15] used the water absorption curve and this model and compared it to histologically observed damage in cornea induced by a single pulse of a tunable (1.8–2.2 μm) Co:MgF_2 laser. It was found that at wavelengths shorter than 1.94 μm, the depth of damage was less than predicted, and at wavelengths longer than 1.94 μm, the depth of damage was larger than predicted using the model. As a reason for this discrepancy, the report speculates that time-dependent changes in optical properties could be responsible.

In dosimetry calculations and in virtually every model that is used for the prediction of the effects of laser radiation, constant optical properties are assumed [16–18]. However, in reality the tissue optical properties often vary in time when energy is deposited into the tissue. Several groups have investigated the dynamics of the optical properties of biological tissues, in particular the irreversible changes of the optical properties due to thermally induced coagulation of tissue components, which is typically associated with cw laser radiation [19–22]. For example, due to thermal denaturation of structural proteins in tissue, the scattering coefficient for visible wavelength increases (a "whitening" of the tissue). As a result, the light distribution is changed [23–25].

Besides the irreversible changes in optical properties, it is also known that the optical properties may change in a reversible fashion. This phenomenon is typically associated with short, high-intensity laser pulses. For example, Pettit et al. [26] in a recent study showed that the scattering in cornea was increased up to 1 ms after a 193 nm ArF laser pulse. In addition, for nonbiological materials such as polyimide films, it has been shown that the optical properties change due to irradiation with UV laser light [27,28]. It was also shown that the absorption coefficient may decrease proportional with the temperature [28].

Water Systems

As early as 1925, changes in the absorption spectrum of liquid water with temperature, without the phase change, were described [29]. It was observed that the water absorption peak at 1.94 μm shifts toward shorter wavelengths as the temperature increases. Since then, several studies have dealt with the infrared optical properties of water and its temperature dependence [30–32]. Recently, it was demonstrated by transmission measurements of picosecond erbium:YAG laser pulses in water, that the absorption coefficient depended on the deposited energy (i.e., temperature) within the absorbing material [33].

Recently, Walsh et al. [34–36] have examined the absorption coefficient of water as a function of energy density at several water absorption peaks and found, e.g., a decrease in the absorption for the erbium:YAG wavelength (λ = 2.94 μm) and a shift to longer wavelength at the 6.1-μm water absorption peak with increasing energy density.

The major change in the absorption coefficient for the midinfrared wavelengths occurs due to the phase change of water into water vapor. As demonstrated for the holmium, thulium, and erbium lasers, for fluences above threshold for water vaporization, the penetration depth can increase up to three orders of magnitude [11–13].

In this report, we focus on the water absorption peak around 1.94 μm, which is important for the absorption of holmium:YAG (λ = 2.12 μm), holmiun:YSGG (λ = 2.09 μm), and thulium:YAG (λ = 2.01 μm) laser light in water and soft tissue. These wavelengths are relevant since several clinically used lasers operate at these wavelengths mainly due to the relatively high absorption in soft tissue and availability of optical fibers that transmit this part of the spectrum. Therefore, in order to investigate the change in the

TABLE 1. Laser Parameters as Used in the Experiments

	λ (μm)	Fiber diameter (μm)	Q/p (mJ)[a]	H (mJ/mm²)[b]
Ho:YAG	2.12	600	10, 20	35.4, 70.7
Ho:YSGG	2.09	950	25	35.3
Tm:YAG	2.01	600	10	35.4

[a]Q/p = laser energy per pulse (mJ/p).
[b]H = radiant exposure (mJ/mm²)

1.94-μm absorption peak of water as a function of temperature, the change in transmission of water with temperature was measured and possible implications are evaluated by means of a model that incorporates the temperature-dependent absorption coefficient.

MATERIALS AND METHODS

Pulsed Laser Experiments

A Schwartz Electro Optics 1-2-3 laser was used to generate Ho:YAG (λ = 2.12 μm), Ho:YSGG (λ = 2.09 μm), and Tm:YAG (λ = 2.01 μm) laser light. The laser beam was coupled into a 600-μm or 950-μm low OH optical fiber. The last centimeter of fiber cladding was removed. The laser was pulsed at 1 pulse per second and the pulse energy was varied from 10 to 25 mJ/p depending on the diameter of the fiber and the wavelength used (Table 1). This range was chosen to avoid water vaporization during the laser pulse and maintain good pulse to pulse stability (variation < 10%). The fiber was placed in a cuvet made out of standard silica-glass microscope slides (Corning) with a thickness of 1 ± 0.05 mm (± range). The cuvet was filled with deionized water. The water temperature was kept constant with a heating element at 22 ± 1, 49 ± 1 or 72 ± 2°C (± range). The temperature of the water was continuously measured with a thermometer in the cuvet and in between laser pulses the temperature in front of the fiber was also measured with a type J (Cu-Con) thermocouple. The water was continuously stirred to ensure a homogenous steady-state temperature throughout the cuvet. At each temperature the transmission was measured as a function of the thickness of the layer of water between the fiber and the bottom of the cuvet using a Joulemeter (Molecton JD-2000). The thickness of the water layer was varied by translating the micrometer to which the fiber was attached. To minimize the effect of the pulse-to-pulse instability of the laser (< 10%) at each thickness of the water layer, the transmission of 40 pulses was measured and the average was determined. A schematic of the setup is shown in Figure 1.

The SEO laser had a variable pulse width option. Part of the laser output (3%) was split off and collected with an IR photodiode (EG&G, Princeton, NJ: Indium-Arsenide J12-18C-R250U, rise time = 1 ns). To monitor the pulse length and pulse structure, the temporal pulse structure was displayed on a oscilloscope. The pulse length used was 200 μs or 1 ms FWHM. A typical 200 μs and 1 ms holmium:YAG pulse structure are shown in Figure 2. Note that the spiky profile and the initial spike that is typically seen with the Ho:YAG laser pulse is absent with the variable pulse width power supply.

To ensure that no water vapor was induced during our study of temperature dependence of absorption properties of liquid water, a time-resolved flash photography setup as described earlier [11] was employed to monitor the interaction of laser pulses with water at the distal end of the fiber during laser pulse delivery. When plotted on a semilogarithmic scale, the curve of percentage transmission versus thickness, z, simply represents Beer's law of attenuation. The slope is the absorption coefficient, μ_a, assuming that $\mu_s' << \mu_a$ (i.e., the effective scattering coefficient is much smaller than the absorption coefficient).

Spectrophotometer Measurements

A Varian Cary 5E UV-Vis-NIR spectrophotometer was used to measure the light transmission through water in the wavelength range from 1,850 to 2,150 nm. A homemade cuvet of regular, 1-mm-thick microscope slides was used. The cuvet was filled with deionized water and the thickness of the water layer was 160 ± 10 μm. A 25-μm-thick type-J thermocouple (Cu-Con) was placed inside the cuvet and the temperature of the water was monitored. The cuvet was heated in a water bath and placed in the spectrophotometer and a transmission scan was made at 22 ± 1, 49 ± 5 and 70 ± 5°C (± range). The sample and optics compartments of the spectrophotometer were purged with nitrogen in order to avoid absorption by water vapor in the air.

Using the Fresnel equation, the transmission data was corrected for reflective losses at the index mismatched interfaces (assuming constant indices of refraction in the wavelength range of interest: $n_{air} = 1$, $n_{water} = 1.31$ and $n_{glass} = 1.51$), and the absorption coefficient was calculated at each temperature. The transmission through a

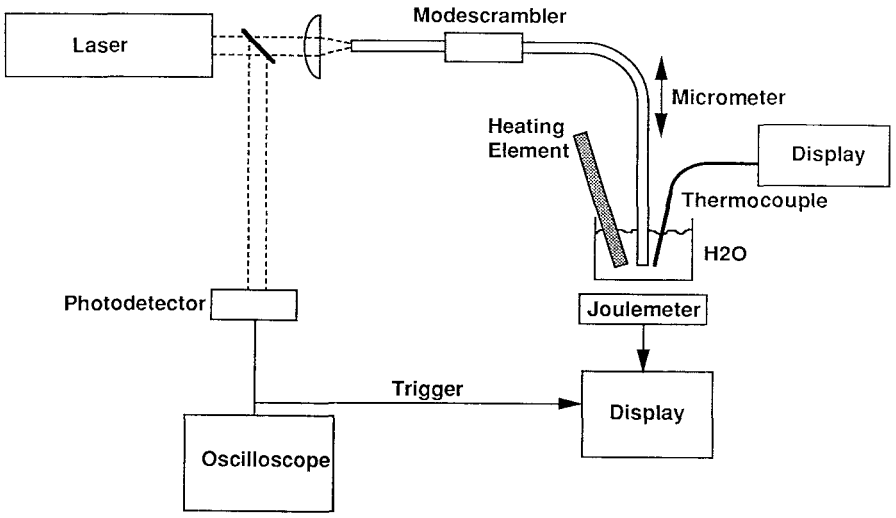

Fig. 1. Schematic of the experimental setup.

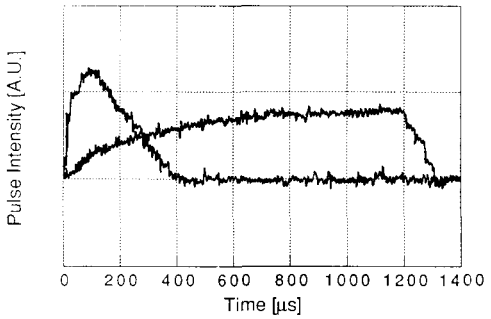

Fig. 2. Temporal beam profile of a 200 μs and 1 ms Ho:YAG laser pulse. The pulse is generated with a SEO 1-2-3 laser with variable pulse width power supply. Note the absence of the initial spike and the spikyness of the pulse that is typically seen with the normal power supply.

microscope slide was measured, and it was determined that the absorption by the microscope slide can be neglected over the wavelength range of interest and that the reflective loss at the surface is constant over the wavelength range.

Model

A computer model was developed that calculated the temperature distribution, incorporating the temperature-dependent absorption coefficient. From the spectrophotometer experiments described above, we established a relationship between the absorption coefficient and the temperature increase. It was assumed that this relationship was linear [37]:

$$\mu_a(T) = \mu_{a,o} + \beta \Delta T \quad (2)$$

where $\mu_a(T)$ is the temperature dependent absorption coefficient [mm^{-1}], $\mu_{a,0}$ is the absorption coefficient at the starting temperature (i.e., room temperature) [mm^{-1}], β is a constant [$mm^{-1}/°C$], and ΔT is the temperature rise above room temperature [°C].

Our spectrophotometer data was curve fitted to find $\mu_{a,0}$ and β, which were then used in the program to calculate the temperature distribution along the z-axis. In the model it was assumed that during the delivery of a pulse of energy no heat conduction and no bubble formation takes place (i.e., the pulse is very short < 20 μs). It was also assumed that the radial beam profile is flat and no divergence of the laser beam takes place in the water. An iterative technique was used, where a small fraction of the energy was deposited and the temperature distribution along the z-axis was calculated. Using equation (2) the values for μ_a along the z-axis were calculated and the next fraction of energy is delivered. The temperature rise due to this was calculated with the new $\mu_a(T)$. This temperature rise was added to the previous temperature rise and we recalculated $\mu_a(T)$. The model uses time steps of 5 ns, assuming a total pulse length of 1 μs and the distance steps were 1 μm, although the model is not very sensitive to variations in either.

RESULTS

Pulsed Laser Experiments

For subablation (i.e., subvaporization) Ho:YAG, Ho:YSGG, and Tm:YAG laser pulses, the

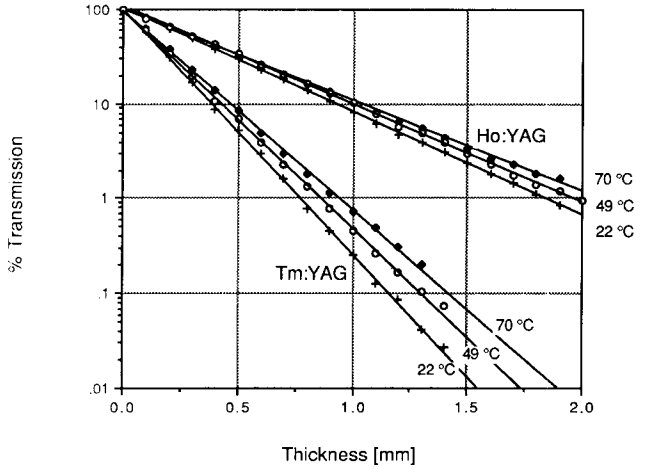

Fig. 3. Semilogarithmic plot of the % transmission of Ho:YAG and Tm:YAG laser pulses through a layer of deionized water with varying thickness at temperatures of 22 ± 1°C (+), 49 ± 1°C (○) and 70 ± 2°C (◆). The laser energy was delivered via a 600 μm fiber. The fluence was 35.4 mJ/mm^2 for the Tm:YAG laser and 70.7 mJ/mm^2 for the Ho:YAG laser.

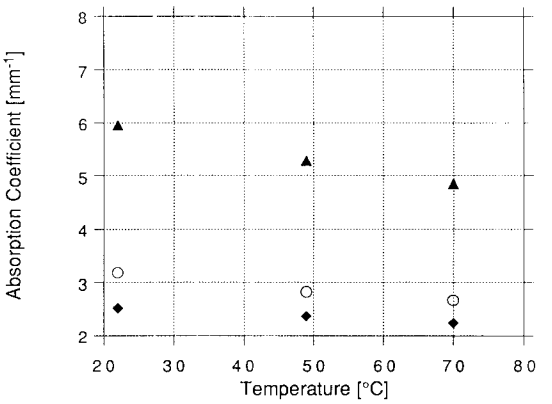

Fig. 4. Absorption coefficient calculated from the pulsed laser experiment as a function of temperature. The lasers used were Ho:YAG (λ = 2.12 μm ◆), Ho:YSGG (λ = 2.09 μm, ○), and Tm:YAG (μ = 2.01 μm, ▲).

transmission through pure deionized water is temperature dependent. In Figure 3 the data points and fitted curves are shown for the Ho:YAG and Tm:YAG transmission at ambient water temperatures of 22 ± 1, 49 ± 1, and 72 ± 2°C. The data for Ho:YSGG transmission is not shown in this graph but falls in between the Ho:YAG and Tm:YAG curves and shows the same trend with increasing water temperature. Note that each data point represents the average of 40 measurements. In all cases the error bars representing the standard deviation were smaller than the symbols. It can be seen that the slope of the curves, i.e., the absorption coefficient, decreases with increasing water temperature. Table 2 shows the absorption coefficients at each temperature for each of the three wavelengths, calculated from the least-squares fit to the data points in Figure 3. The absorption coefficients as inferred from the laser experiments are plotted as a function of temperature in Figure 4.

The calculated absorption coefficient for the Ho:YAG and Tm:YAG laser pulses at any temperature did not change significantly from a 200 μs to a 1 ms pulse duration. The fast flash photography setup did not reveal any bubble formation at the end of the fiber tip. Even in the case where bubble formation would be most likely, in 72°C water using the Tm:YAG laser with 10 mJ/p (35.7 mJ/mm^2), no bubble formation was observed.

Spectrophotometer Measurements

Figure 5 shows the absorption spectra from 1,850 to 2,150 nm for water at 22 ± 1, 49 ± 5, and 70 ± 5°C. It can be seen that with increasing temperature, the absorption peak shifts toward shorter wavelengths (from 1,938 nm at 22°C to 1920 nm at 70°C), and the peak absorption coefficient increases slightly. Since the wavelengths of Tm:YAG, Ho:YSGG, and Ho:YAG all fall on the right side of the absorption peak, the absorption coefficients of all three wavelengths drop with temperature as can be seen in Figure 6. The values of the absorption coefficient for the wavelengths corresponding to the three laser wavelengths are shown in Table 2. The minimum and maximum values correspond to 150-μm and 170-μm thick cuvettes.

Model

By curve fitting the absorption coefficients from the spectrophotometer data to the temperature rise (Fig. 6), values for the abscissa ($\mu_{a,0}$) and the slope (β) in equation (3) were obtained. The values obtained for $\mu_{a,0}$ and β at 2.01 μm, 2.09 μm, and 2.12 μm are shown in Table 3. Using these coefficients, the computer program was used to calculate the temperature distribution along the z-axis at different radiant exposures. In Figure 7 the results are shown for Ho:YAG and Tm:YAG pulses of 10, 50, and 100 mJ with a variable, temperature-dependent μ_a and with a constant μ_a. In all cases the initial temperature of the water was 22°C (temperature rise = 0°C). It can be seen that the change in absorption coefficient

TABLE 2. Calculated Absorption Coefficients in Relation to Temperature (T)*

Laser-experiments				Spectrophotometer			
T (°C)	Ho:YAG 2.12 μm	Ho:YSGG 2.09 μm	Tm:YAG 2.01 μm	T (°C)	2.12 μm	2.09 μm	2.01 μm
22 ± 1	2.51	3.18	5.95	22 ± 1	2.80–3.18	3.46–3.92	6.97–7.90
49 ± 1	2.36	2.82	5.28	49 ± 5	2.61–2.96	3.17–3.59	6.38–7.23
72 ± 2	2.23	2.66	4.84	70 ± 5	2.41–2.74	2.87–3.25	5.51–6.24

*These values were calculated from the transmission experiments with the lasers (left side) or from the spectrophotometer data (right side). The range on the right side represents the uncertainty in the thickness of the cuvet (150–170 μm).

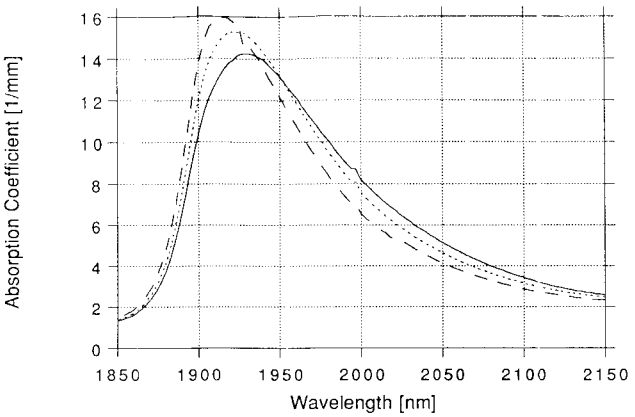

Fig. 5. Water absorption spectra at three different temperatures through a cuvet of 160 ± 10 μm of thickness, recorded with a spectrophotometer. Water temperature was 22 ± 1°C (solid line), 49 ± 5°C (dotted line) or 70 ± 5°C (striped line).

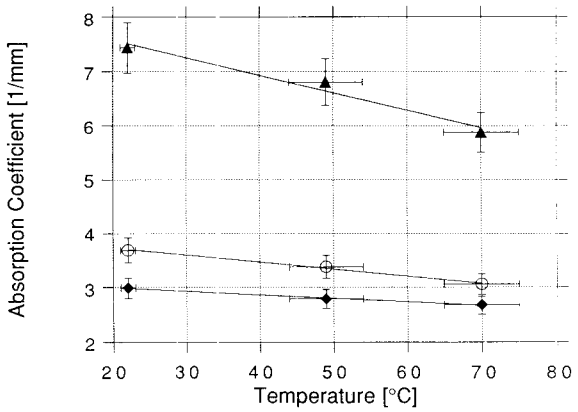

Fig. 6. At λ = 2.12 μm, λ = 2.09 μm and λ = 2.01 μm, the absorption coefficients were calculated from the spectrophotometer data. The horizontal error bars represent the uncertainty in temperature and the vertical error bars represent the uncertainty in the thickness of the cuvet. The linear curve fit was used to determine $\mu_{a,0}$ and β (Table 3), which were used in the computer model.

has a significant impact on the temperature distribution.

DISCUSSION

In this study we examined the reversible change of the absorption coefficient of water due to an increase in temperature. Although all experiments were done in pure water, we believe that the results are also an indication for what will happen when soft tissue is irradiated with infrared laser light, since soft tissue is > 70% water and water is the main absorber for the midinfrared wavelengths.

The shift of water absorption peak at 1.94 μm can be described using the spectroscopy of water. The absorption peaks are the result of absorption of radiation by the fundamental stretching and bending vibrations of OH bonds in the water molecule, their overtones and combinations of the fundamentals and overtones [30,31]. In addition, the environment of the water molecule has an influence on its infrared optical behavior. For example, liquid water forms a hydrogen-bond network. As a result, the vibration modes will be shifted to lower frequencies. The temperature dependence of the absorption peak can also be described in terms of the temperature effect on the hydrogen-bond network. It has been suggested that an increase in temperature weakens the hydrogen-bond network structure [30,38,39]. However, a detailed review of this theory is beyond the scope of this report.

It has been shown that the H-bonding structure can be affected by temperature changes on a picosecond time scale [33,40]. "Long-lived" spectral changes become prominent after 50 ps; the time needed for an equilibration of translational, rotational, and vibrational modes after excitation with a picosecond IR pulse. Relative to the pulse length used in our experiments, the time constants associated with equilibration are negligible and the temperature rise can be considered instantaneous. This explains why no difference was seen between the absorption coefficient values we obtained using 200 μs and 1 ms pulses with the same energy.

TABLE 3. Values for $\mu_{a,0}$ and β at 2.12, 2.09, and 2.01 μm Wavelength, Derived From the Linear Curve Fit of the Spectrophotometer Data (Fig. 6)*

	2.12 μm	2.09 μm	2.01 μm
$\mu_{a,0}$ [mm^{-1}]	2.982	3.703	7.507
β [mm^{-1}/°C]	−0.00661	−0.01305	−0.03207
$\Delta\mu_a$ (20–>100°C)	18%	28%	34%
r^2	0.97	0.99	0.99

*Also given are the r^2 values of the curve fit. Note that the $\mu_{a,0}$ values are given for room temperature (22°C). For the model it is assumed that at room temperature the temperatures rise, ΔT = 0°C.

Reflective Losses

The importance of Fresnel reflections at water–glass and air–glass interfaces was analyzed for both our laser and spectrophotometer experiments. In the pulsed laser experiments the measurements we made were of the transmission versus change in path length at each temperature. Although losses at the interfaces are likely to produce an offset of the transmission versus thickness curves, the slope, which gives us the values for the absorption coefficient, is unaffected by these reflective losses.

For the spectrophotometer results, the situation was slightly more complicated. The transmission spectrum of a single microscope slide in air revealed that 92.1 ± 0.2% of the incident light was transmitted over the entire wavelength range from 1.8–2.2 μm. The theoretical transmission, considering only reflective losses at the surface was 92.16%. Hence we assumed that the glass did not absorb 1.8–2.2 μm radiation. The second issue in analyzing the spectrophotometer data is the fact that the index of refraction of water is known to change with temperature [37]. However, it was stated that for temperatures within 50°C of the tabulated values that are found in the literature (at room temperature) the change in refractive index can be neglected. In our spectrophotometer results the percentage transmission was corrected for one air–glass, one glass–water, one water–glass, and one glass–air interface, assuming temperature independent indices of refraction.

Implications of Dynamic Absorption Coefficient

The consequences of the variation of the absorption coefficient as a function of temperature are significant. First, the measurement of absorption coefficient can be influenced by the probing beam itself. This is the case in our experiment with the transmission of the three different laser wavelengths; on top of the preset ambient water temperature the laser pulse itself heats up the water and influences the absorption coefficient. As was shown with the model (Fig. 7), a pulse of only 10 mJ of Tm:YAG radiation delivered via a 600 μm fiber increases the temperature up to 50°C just in front of the fiber assuming an initial temperature of 22°C. This may also be an explanation for the discrepancy in absorption coefficients we obtained with the pulsed laser and the spectrophotometer. The lower values obtained from the laser experiments are likely underestimated since the temperature is increased by the absorbed energy of the probing beam. In contrast, the energy delivered to the water cuvet by the beam in the spectrophotometer is so low (< 1 mW) that temperature rise in that case may be neglected. Hence, the probing beam energy is an important parameter to know, when interpreting transmission data.

When comparing our spectrophotometer data to other data in the literature, we noted that in general the values and trends correspond well [29,37,41]. Similar to Collins [29] who mainly was interested in the behavior of the water absorption curve as a function of temperature, we observed a shift to shorter wavelength of the 1.94 μm absorption peak of water as well as an increase in the peak value. Comparing the absolute values of the absorption coefficient that we found to Collins and Curcio's data at room temperature, we noted that the values, especially those close to the absorption maximum at 1.94 μm, are slightly higher. For example, Curcio found a maximum absorption coefficient at 1.94 μm of 11.4 mm^{-1} while we found a maximum at the same wavelength of 14.2 mm^{-1}. Neither Curcio or Collins mentioned the power of the probing beam, hence bleaching due to absorption of the probing beam itself may interfere with their results. We speculate that this discrepancy may be due to the fact that with current advances in optical and detector technology more sensitive measurements can be made and lower power probing beams may be used.

Another observation that deserves an explanation is the fact that no bubble formation was observed during the pulsed laser experiments, not even during irradiation with the most strongly absorbed, Tm:YAG wavelength in water of 70°C. Theoretically a 60°C increase in temperature (assuming constant μ_a = 7.50 mm^{-1}) on top of a 70°C starting temperature would give rise to at

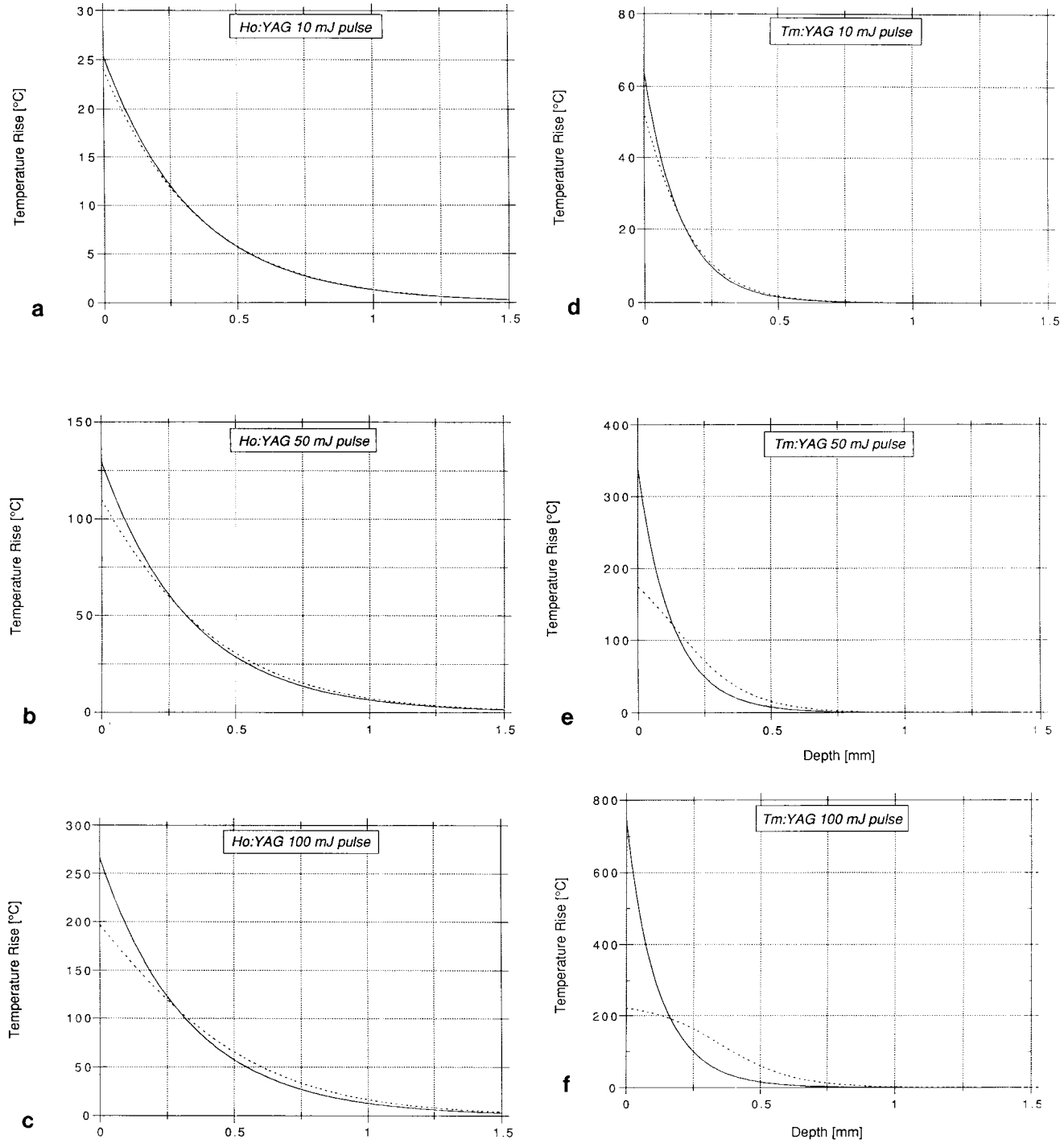

Fig. 7. Temperature distribution in water along the z-axis with constant (solid line) and with dynamic μ_a (dotted line) used in the model. It is assumed that there is no heat conduction, no bubble formation, no beam divergence, and a block pulse of laser energy going in. The model also assumes a 600-μm diameter spot size. (**a**) Ho:YAG pulse, 10 mJ (35.4 mJ/mm^2); (**b**) Ho:YAG pulse, 50 mJ (177 mJ/mm^2); (**c**) Ho:YAG pulse, 100 mJ (354 mJ/mm^2); (**d**) Tm:YAG pulse, 10 mJ (35.4 mJ/mm^2); (**e**) Tm:YAG pulse, 50 mJ (177 mJ/mm^2); (**f**) Tm:YAG pulse, 100 mJ (354 mJ/mm^2).

least some water vaporization, although it would not be much since the latent heat of vaporization still needs to be delivered in order to vaporize water. We have seen in a previous study that only a very small fraction of the actual heat of vaporization is needed for vaporization [42]. The explana-

tion can be found in the fact that the starting temperature of the water is already 70°C and consequently the absorption coefficient is reduced. Using the model, it was calculated that the temperature rise would only be 40°C. Although this would still lead to a cumulative temperature of 110°C in the few μm just in front of the fiber, apparently there is not enough energy available to vaporize enough water molecules to create a visible water vapor bubble.

As shown in Figure 7, the fact that the absorption coefficient changes with temperature has important consequences for the temperature distribution in water. In the model we assumed no heat conduction, no bubble formation, a flat radial beam profile, and no divergence in the water. This is representative for the situation that occurs, for example, when a short holmium:YAG laser pulse is delivered in soft tissue. The model gives the temperature distribution at the moment before heat conduction takes place and before water vaporization starts. The thermal diffusion time is typically on the order of several tens of milliseconds for the Ho:YAG and Tm:YAG wavelengths. Hence temperatures of superheated water of up to 700°C are not unreasonable. However, in our model we have assumed a linear relation between the absorption coefficient and the temperature increase. For the temperature range in our experiments, this seems to be a reasonable assumption, but it is not known to what extent this linearity holds at higher temperatures, especially > 100°C. The result of the temperature-dependent absorption is that the depth of penetration increases significantly. For example, when a 100 mJ thulium:YAG pulse is delivered, the depth to which water is heated to 100°C is increased from 250 μm to 390 μm when a temperature-dependent absorption coefficient is considered compared to a constant value for μ_a. Similarly, the depth to which thermal damage occurs increases significantly with the variable absorption coefficient. It has been shown that thermal denaturation of collagen takes place at a temperature of ~ 58°C [25]. Consequently, an increase in the depth to which this temperature is reached will likely result in a larger thermal damage zone. For example, in photo refractive surgery, where cw midinfrared lasers are used for hyperopia correction, a larger zone of damage could be very critical to Descemet's membrane [6,43].

An excellent illustration of the effect of changes in absorption coefficient can be found when we refer to the report of Schomacker et al. [15]. As noted in the Introduction, he found more thermal damage than expected using wavelengths longer than 1.94 μm, whereas the damage was smaller than expected using wavelengths shorter than 1.94 μm. The expected damage was based on a simple model that used the depth to which the tissue was heated to a critical temperature. This depth is inversely proportional to the absorption coefficient, assuming negligible scattering. From the results presented in our study, we know that the absorption coefficient decreases for wavelengths longer than 1.94 μm since the peak shifts to shorter wavelengths. As a consequence, the penetration depth (i.e., damage depth) increases for wavelengths longer than 1.94 μm. In contrast, at wavelengths shorter than 1.94 μm, the absorption increases resulting in a smaller penetration depth. This is in excellent agreement with Schomacker's data.

Although the change in absorption coefficient of water in the liquid state is important as we have shown, it should be kept in mind that in most ablative applications of midinfrared lasers bubble formation (i.e., explosive vaporization process) will take place [11]. Once water becomes water vapor, a much more dramatic change in absorption coefficient takes place (up to 3 orders of magnitude) [11–13,44]. The change in absorption coefficient in the liquid state will also influence the threshold fluence for vaporization. The threshold fluence for vaporization of water, H_{th} depends on the absorption coefficient and is generally described as:

$$H_{th} = \frac{\rho\,(c\,\Delta T + L_v)}{\mu_a} \qquad (3)$$

where ρ is the density [g/mm^3], c is the specific heat [J/g °C], ΔT [°C] is the difference between the initial temperature, T_0, and the boiling temperature of water, T_b, L_v is the latent heat of vaporization [J/g], and μ_a is the absorption coefficient [mm^{-1}]. Therefore, a decrease in μ_a, as occurs for the holmium and thulium laser wavelengths, will increase the threshold fluence for vaporization. This may also be important during multiple pulse delivery. We have shown in another study [45] that the baseline temperature during consecutive laser pulses does not return to its initial value in between pulses. This thermal superposition will affect the starting value for the absorption coefficient at the start of each laser pulse, thus causing

deeper damage and lower ablation efficiencies than expected.

In conclusion, the water absorption peaks around 1.94 μm, which is important for the absorption of holmium, and thulium laser radiation, shifts to shorter wavelengths when the temperature increases. This phenomenon takes place during pulsed laser delivery and has important consequences for the effective absorption coefficient at these wavelengths. In order to accurately predict damage depths and ablation related parameters, the dynamics of μ_a need to be incorporated in models and dosimetry calculations.

ACKNOWLEDGMENTS

The authors gratefully acknowledge the support of the Office of Naval Research (grant N00014-91-J-1564), the Albert and Clemmie Caster Foundation, the Netherlands Heart Foundation (grant 37.007), and the National Science Foundation (grant BCS-9110257). We thank Dr. Ed Sinofsky of Rare Earth Medical for his advice concerning the IR lasers.

REFERENCES

1. White CJ, Ramee SR, Collins TJ, Mesa JE, Paulsen DB, Murgo JP. Recanalization of arterial occlusions with a lensed fiber and a holmium:YAG laser. Lasers Surg Med 1991; 11:250–256.
2. Haase KK, Baumbach A, Wehrmann M, Duda S, Cerullo G, Ruckle B, Steiger E, Karsch KR. Potential use of holmium lasers for angioplasty: Evaluation of a new solid-state laser for ablation of atherosclerotic plaque. Lasers Surg Med 1991; 11:232–237.
3. Trauner K, Nishioka N, Patel D. Pulsed holmium:yttrium-aluminum-garnet (Ho:YAG) laser ablation of fibrocartilage and articular cartilage. Am J Sports Med 1990; 18:316–320.
4. Black JD, Sherk HH, Rodes ALB, Smith RC. Anterior cervical discectomy using Holmium:YAG laser. Surgical Forum 1990; 41:527–530.
5. Gottlob C, Kopchok GE, Pemg SK, Trabbara M, Cavaye D, White RA. Holmium:YAG laser ablation of human intervertebral disc: Preliminary evaluation. Lasers Surg Med 1992; 12:86–91.
6. Seiler T, Matallana M, Bende T. Laser thermokeratoplasty by means of a pulsed holmium:YAG laser for hyperopic correction. Refractive & Corneal Surg 1990; 6:335–339.
7. Shapshay SM, Rebeiz EE, Bohigian RK, Hybels RL, Aretz HT, Pankratov MM. Holmium: yttrium aluminum garnet laser-assisted endoscopic sinus surgery: Laboratory experience. Laryngoscope 1991; 101:142–149.
8. Schlenk F, Profeta G, Nelson JS, Andrews JA. Laser assisted fixation of ear prosthesis after stapedectomy. Lasers Surg Med 1990; 10:444–447.
9. Izatt JA, Albagli D, Itzkan I, Feld MS. Pulsed laser ablation of calcified tissue: Physical mechanisms and fundamental parameters. In: Jacques SL and Katzir A, eds. "Laser-Tissue Interaction I." Bellingham: SPIE, 1990, pp. 133–140.
10. van Leeuwen TG, van Erven L, Meertens JH, Motamedi M, Post MJ, and Borst C. Origin of arterial wall dissections induced by pulsed excimer and mid-infrared laser ablation in the pig. J Am Coll Cardiol 1992; 19:1610–1618.
11. van Leeuwen TG, van der Veen MJ, Verdaasdonk RM, Borst C. Non-contact tissue ablation by holmium:YSGG laser pulses in blood. Lasers Surg Med 1991; 11:26–34.
12. Loertscher H, Shi WQ, Grundfest WS. Tissue ablation through water with erbium:YAG lasers. IEEE Trans Biomed Eng 1992; 39:86–87.
13. Lin CP, Stern D, Puliafito CA. High-speed photography of Er:YAG laser ablation in fluid: Implication for vitreous surgery. Invest Ophthalmol Vis Sci 1990; 31:2546–2550.
14. Parsa P, Jacques SL, Nishioka NS. Optical properties of rat liver between 350 and 2200 nm. Appl Optics 1989; 28:2325–2330.
15. Schomacker KT, Domankevitz Y, Flotte TJ, Deutsch TF. Co:MgF2 laser ablation of tissue: Effect of wavelength on ablation threshold and thermal damage. Lasers Surg Med 1991; 11:141–151.
16. Walsh JT Jr., Deutsch TF. Er:YAG laser ablation of tissue: Measurements of ablation rates. Lasers Surg Med 1989; 9:327–337.
17. Gijsbers GH, Selten FM, van Gemert MJC. CW laser ablation velocities as a function of absorption in an experimental one-dimensional tissue model. Lasers Surg Med 1991; 11:287–296.
18. Furzikov NP. Model and description of UV laser ablation of the cornea. In: Jacques SL and Katzir A, eds. "Laser-Tissue Interaction I." Bellingham: SPIE, 1990, pp. 286–298.
19. Agah R, Motamedi M, Dalmia P. Changes in optical constants of thermally damaged arterial tissue as a function of wavelength. Lasers Surg Med 1990; suppl:2 (52): 15.
20. Gourgouliatos ZF. Behavior of optical properties of tissue as a function of temperature. Masters thesis, Univ of Texas, Austin, 1986.
21. Rastegar S, Kim BM, Jacques SL. Role of temperature dependence of optical properties in laser irradiation of biological tissue. in Jacques SL and Katzir A, eds. "Laser-Tissue Interaction III." Bellingham: SPIE, 1992; pp. 228–231.
22. Splinter R, Svenson RH, Littmann L, Tuntelder JR, Chuang CH, Tatsis GP, Thompson M. Optical properties of normal, diseased, and laser photocoagulated myocardium at the Nd:YAG wavelength. Lasers Surg Med 1991; 11:117–124.
23. Jacques SL. Laser-tissue interactions: Photochemical, photothermal and photomechanical. Surg Clin Am 1992; 72:531–558.
24. van Gemert MJC, Welch AJ, Jacques SL, Cheong WF, Star WM. Light distribution, optical properties, and cardiovascular tissues. In Abela GJ ed: "Lasers in Cardiovascular Medicine." New York, Wolters Nijhoff, 1990, pp. 93–110.
25. Thomsen S. Pathologic analysis of photothermal and photomechanical effects of laser-tissue interactions. Photochem Photobiol 1991; 53:825–835.

26. Pettit GH, Ediger MN. Pump/probe transmission measurements of corneal tissue during excimer laser ablation. Lasers Surg Med 1993; 13:363–367.
27. Pettit GH, Sauerbry R. Fluence-dependent transmission of polyimide at 248 nm under laser ablation conditions. Appl Phys Lett 1991; 58:793–795.
28. Frisoli JK, Hefetz Y, Deutsch TF. Time-resolved UV absorption of polyimide-implications for laser ablation. Appl Phys B 1991; 52:168–172.
29. Collins JR. Change in the infrared absorption spectrum of water with temperature. Phys Rev 1925; 26:771–779.
30. Hale GM, Querry MR, Rusk AN, Williams D. Influence of temperature on the spectrum of water. J Opt Soc Am 1972; 62:1103–1108.
31. Pinkley LW, Sethna PP, Williams D. Optical constants of water in the infrared: influence of temperature. J Opt Soc Am 1977; 67:494–499.
32. Falk M, Ford TA. Infrared spectrum and structure of liquid water. Can J Chem 1966; 44:1699–1707.
33. Vodopyanov KL. Saturation studies of H2O and HDO near 3400/cm using intense picosecond laser pulses. J Chem Phys 1991; 94:5389–5393.
34. Cummings JP, Walsh JT. Thermal changes in the absorption spectrum of water near 6.1 μm. Lasers Surg Med 1993; suppl.5 (7): 2.
35. Walsh JT. personal communication (1992/1993).
36. Cummings JP, Walsh JT. Erbium laser ablation: The effect of dynamic optical properties. Appl Phys Lett 1993; 62:1988–1990.
37. Irvine WM, Pollack JB. Infrared optical properties of water and ice spheres. Icarus 1968; 8:324–360.
38. Bandekar J, Curnutte B. The intramolecular vibrations of the water molecules in the liquid state. J Mol Spectrosc 1972; 41:500–511.
39. Bryan JB, Curnutte B. A normal coordinate analysis based on the local structure of liquid water. J Mol Spectrosc 1972; 41:512–533.
40. Graener H, Seifert G, Laubereau A. New spectroscopy of water using tunable picosecond pulses in the infrared. Phys Rev Lett 1991; 66:2092–2095.
41. Curcio JA, Petty CC. The near infrared absorption spectrum of liquid water. J Opt Soc Am 1951; 41:302–304.
42. van Leeuwen TG, Jansen ED, Motamedi M, Borst C, Welch AJ. Excimer laser ablation of soft tissue: A study of the content of fast expanding and collapsing bubbles. IEEE J Quantum Electron (in press).
43. Smithpeter CL, Welch AJ, Rylander III HG. Evaluation of a unique cw holmium laser in radial thermokeratoplasty. In Parel JM, Ren O, Katzir A eds. "Ophthalmic Technologies III." Bellingham: SPIE, (in press).
44. van Leeuwen TG, Motamedi M, Verdaasdonk RM, Borst C. Interaction of pulsed IR laser radiation with fluid: implication for tissue ablation. Lasers Surg Med 1991; suppl: 3: 16–16.
45. Jansen ED, Le TH, Welch AJ. Excimer, Ho:YAG and Q-switched Ho:YAG ablation of aorta: A comparison of temperatures and tissue damage in vitro. Appl Optics 1993; 32:526–534.